

The Catalytic Mechanism of RNA Polymerase II

Alexandra T. P. Carvalho, Pedro A. Fernandes, and Maria J. Ramos*

Requimte, Faculty of Sciences of Porto, Rua do Campo Alegre S/N, 4169-007 Porto, Portugal

 Supporting Information

ABSTRACT: Eukaryotic RNA polymerase II (RNAP II) transcribes the DNA into mRNA. The presence of two metal ions (usually Mg^{2+}) and conserved aspartate residues in the active sites of all nucleic acid polymerases led to the adoption of a universal catalytic mechanism, known as the “two metal ion catalysis”. In this scheme, it is assumed that the coordination shell of Mg^{2+} (geometry, number, and identity of the ligands) is basically the same for all of the enzymes, despite the significant differences in sequence and structure commonly found in multisubunit RNA polymerases versus single-subunit RNA polymerases and DNA polymerases. Here, we have studied the catalytic mechanism of RNAP II and found very interesting variations to the postulated mechanism. We have used an array of techniques that included thermodynamic integration free energy calculations and electronic structure calculations with pure DFT as well as hybrid DFT/semiempirical methods to understand this important mechanism. We have studied four different catalytic pathways in total, resulting from different combinations of proton donors/acceptors for the two proton transfers experimentally detected (deprotonation of the 3' hydroxyl of the terminal nucleotide (HO_{RNA}) and protonation of pyrophosphate). The obtained data unambiguously show that the catalytic mechanism involves the deprotonation of HO_{RNA} by a hydroxide ion coming from the bulk solvent, the protonation of pyrophosphate by the active site His1085, and the nucleophilic attack to the substrate by O^{-}_{RNA} . The overall barrier is 9.9 kcal/mol. This mechanism differs from those proposed in the identity of the general acid. The deprotonation of the HO_{RNA} and the transition state for the nucleophilic attack are similar to some (but not all) of the family members.

1. INTRODUCTION

Two different evolutive solutions have emerged for transcription: The first corresponds to a large family of multisubunit RNAPs, which includes bacterial enzymes and eukaryotic nuclear enzymes (RNAP I, RNAP II, and RNAP III), among others. The second involves single-subunit RNAPs that include enzymes from bacteriophages, such as T7 RNAP, among others. Single-subunit RNAPs share a strong structural homology to DNA polymerases (DNAPs).

This work deals with RNAP II, which is the multisubunit eukaryotic RNA polymerase responsible for the transcription of the genomic DNA into mRNA in eukaryotic cells. It consists of a 10-subunit catalytic core and a heterodimeric Rpb4/7 subcomplex. The active site is located in the interface between the core subunits Rpb1 and Rpb2 and contains two Mg^{2+} ions (Figure 1). According to Wang et al. for RNAP II, one is a persistently bound Mg^{2+} (the catalytic magnesium, Mg_A^{2+}).¹ The second Mg^{2+} (the nucleotide-binding magnesium, Mg_B^{2+}) is only found in the transcribing complex with the substrate. There is not a general mechanism for how Mg^{2+} binding happens during the catalytic cycle of polymerases, and such a general mechanism may not exist at all. In fact, for DNA polymerase β , both ions are believed to leave the active site after the catalytic reaction and to re-enter for the new cycle.

The ions are held in place through coordination to four aspartates (Asp481, Asp483, Asp485, and Asp837) and the triphosphate of the substrate.¹ The enzyme has a very flexible motif at the active site (the trigger loop) that closes the active site upon substrate (NTPs) binding.¹

The four-step cyclic process of nucleotide addition first involves the selection of a specific NTP. This occurs in two

phases, with an initial binding to the entry site, in an inverted orientation, followed by rotation to the nucleotide addition site, for pairing with the complementary template DNA. In the second step, the very flexible trigger loop suffers a conformation change and closes the active site. The catalyzed phosphodiester bond formation follows, and finally, translocation finishes the cycle.

The reaction mechanism is postulated to be common to all nucleic acid polymerases. It involves a nucleophilic attack by O^{-}_{RNA} to the phosphorus atom of the α phosphate of the substrate (P_α), forming a new phosphodiester bond and releasing pyrophosphate (PPi; see Schemes 1 and 2). For this reaction to be accomplished, two proton transfers must also take place: HO_{RNA} must be deprotonated, and PPi must be protonated, as it is known to be released in the monoprotonated form.^{2,3} The general scheme does not explain the first proton transfer. The protonation of PPi is also not addressed in the general two ion catalytic scheme. Therefore, the HO_{RNA} proton acceptor and PPi proton donor are presently unknown. Three hypotheses are advanced for the identity of the base that deprotonates HO_{RNA} in DNA polymerases (DNAPs). The first corresponds to a suitable protein residue, namely, the catalytic triad Asp closer to the DNA terminus.^{4–6} In RNAP II, it corresponds to Asp485. In the second hypothesis, the base is one of the two nonbridging α -oxygens of the substrate ($O\alpha$).^{7,8} The third hypothesis is a HO^- ion coming from the bulk solution (the external HO^- hypothesis).^{6,9,10} This last hypothesis was first proposed for the

Received: October 8, 2010

Published: March 18, 2011

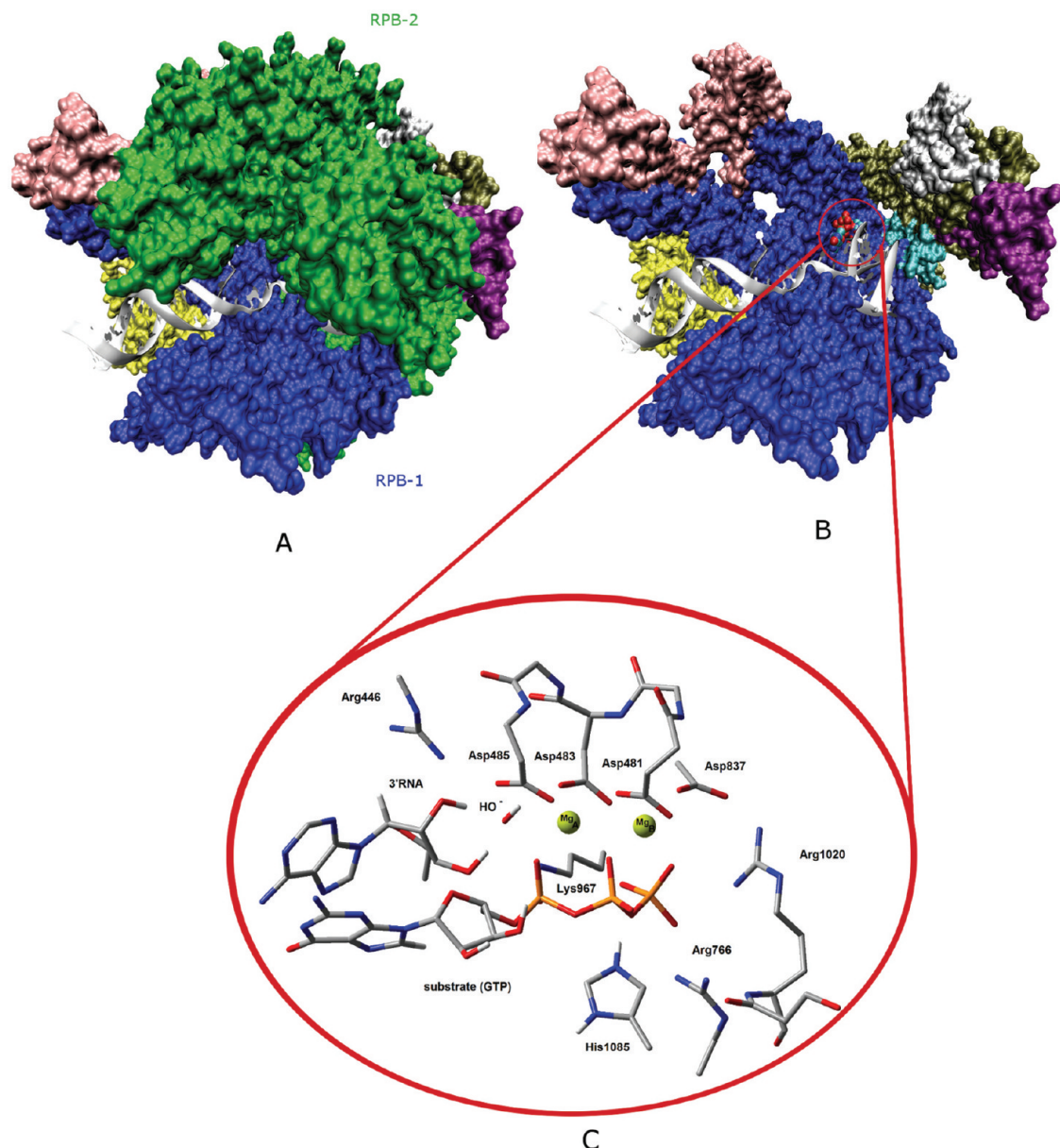
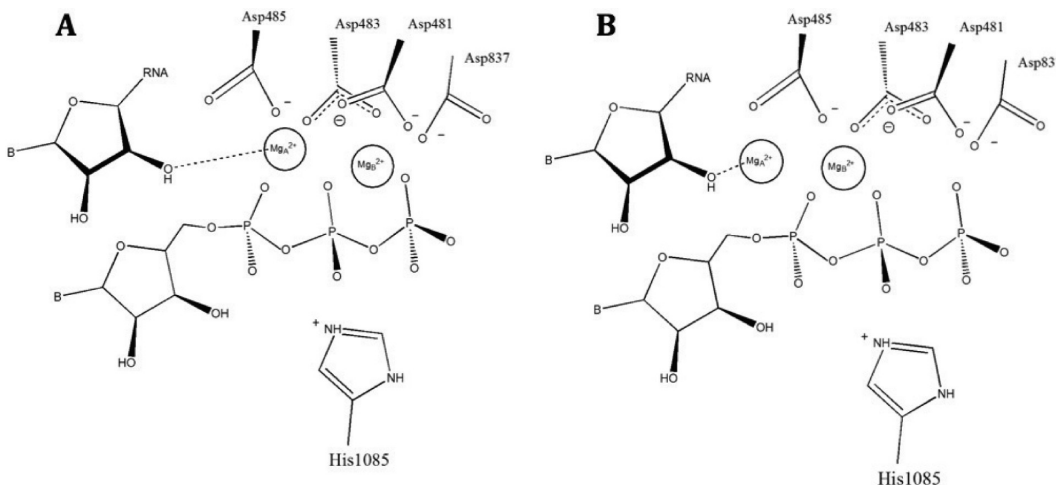


Figure 1. The RNAP II structure. (A) The overall complex protein-DNA.RNA.substrate. (B) The same structure with the Rpb-2 deleted so that the active site (VDW representation) and DNA.RNA hybrid can be seen. (C) The atoms of the active site included in the DFT calculations. Each model contains the substrate (GTP); the 3' terminal nucleotide of the RNA chain; the two magnesium ions; the aspartates 481, 483, 485, and 837; the protonated histidine 1085; the arginines 446, 766, and 1020; and Lys967. Some of the models also included a HO^- ion. Most of the hydrogen atoms were deleted in the figure for simplicity.

exonuclease reaction of DNA polymerase I¹¹ and later by Flórian et al.⁶ for the polymerization reaction by T7 DNA polymerase. Flórian et al. estimated that the free energy required for the hydroxide to deprotonate the HO_{RNA} at neutral pH was in the range of 1.5–3.0 kcal/mol.¹⁰ On the basis of the similarity between the active sites of RNAP II and DNAPs, it seems logical to consider the same hypothesis for the deprotonation of HO_{RNA} .

Recently, the protonation of the leaving PPi by a protein residue was proposed.² This assumption was based on a proton-inventory experiment. The data were consistent with a model in which more than one proton transfer occurred during a nucleotidyl transfer reaction. Subsequently, to check this hypothesis,

nucleotide incorporation rates were measured for four representatives of the four classes of nucleic polymerases (the RNA-dependent RNA polymerase from poliovirus (PV), the reverse transcriptase (RT) from human immunodeficiency virus type 1, the DNA-dependent DNA polymerase from bacteriophage RB69, and the DNA-dependent RNA polymerase from bacteriophage T7). It was concluded that the polymerases employ a general acid catalysis mechanism for nucleotidyl transfer. Importantly, the general acid is not absolutely essential but provides a 50–2000 fold rate enhancement depending upon the polymerase evaluated.³ Multisubunit RNA polymerases contain a histidine in the trigger loop that can serve as a general acid.¹ Changing His1085 to Tyr reduces the rate of catalysis by an order

Scheme 1. The Position of the Mg^{2+} Ions in the MD Simulations (A) and in the Two Metal Ions Catalysis Scheme (B)

of magnitude without changing the observed affinity for the nucleotide substrate,¹² which is fully consistent with the above-mentioned results and points to His1085 as a candidate for the role of acid in the general acid catalysis mechanism.

The two active site Mg^{2+} ions participate actively in catalysis. The two-metal ion catalysis scheme was first described 20 years ago, upon the determination of the crystallographic structure of the exonuclease active site of DNA polymerase I.¹³ The hypothesis was later applied to RNA splicing, hydrolysis of tRNA by RNase P, and several DNA polymerases.^{14,15} All of these mechanistic proposals were essentially based on the observation of the crystallographic structures of the mentioned enzymes. Mg_A^{2+} is thought to orient and activate the nucleophile (here, HO_{RNA}). Activation is achieved through the lowering of the pK_a of the nucleophile, facilitating its deprotonation. Mg_B^{2+} is thought to stabilize the negative charge that develops in the postulated pentacoordinated transition state and facilitate the leaving of PPi .¹⁴

If these mechanisms are correct, this would be a clear case of convergent evolution. A myriad of structurally unrelated enzymes, involved in phosphoryl transfer reactions, would employ the same two-ion mechanism to accomplish their roles.

The ions seem to be essential for substrate recognition and for the greater specificity of the enzymes. The reported distance between the metal ions in most polymerases is around 4 Å. However the positions and distance of the metals may change at each reaction step due to differences in the coordination environment. Yang et al. hypothesized that the conformation with the metals separated by 4 Å should represent a “resting state” and that during the reaction Mg_A^{2+} should move toward Mg_B^{2+} , bringing the nucleophile within striking distance for phosphoryl bond formation.¹⁶ The approximation of the Mg^{2+} ions could also better neutralize the developing negative charge on the pentacovalent intermediate.¹⁶

The purpose of the present study is to identify the elementary steps that constitute the catalytic pathway, quantifying the activation barriers and reaction energies, characterizing the transition states, and finally elucidating and understanding the mechanism by which RNAP II catalyzes the biosynthesis of the mRNA.

To fulfill our goal, we have used several techniques, namely molecular dynamics (MD), thermodynamic integration (TI) free

energy calculations, density functional theory (DFT), and hybrid quantum mechanics/molecular mechanics (QM/MM) methods, more precisely DFT:PM3MM.

We have explored four different mechanistic hypotheses that differed mostly in the proton transfer reactions. The results allowed for the identification and understanding of the catalytic mechanism of RNAP II, which is in fact different from those proposed in the literature as far as the identity of the general acid is concerned. Furthermore, the protonation of the HO_{RNA} and the transition state for the nucleophilic attack are similar to some, albeit not all, of the family members.

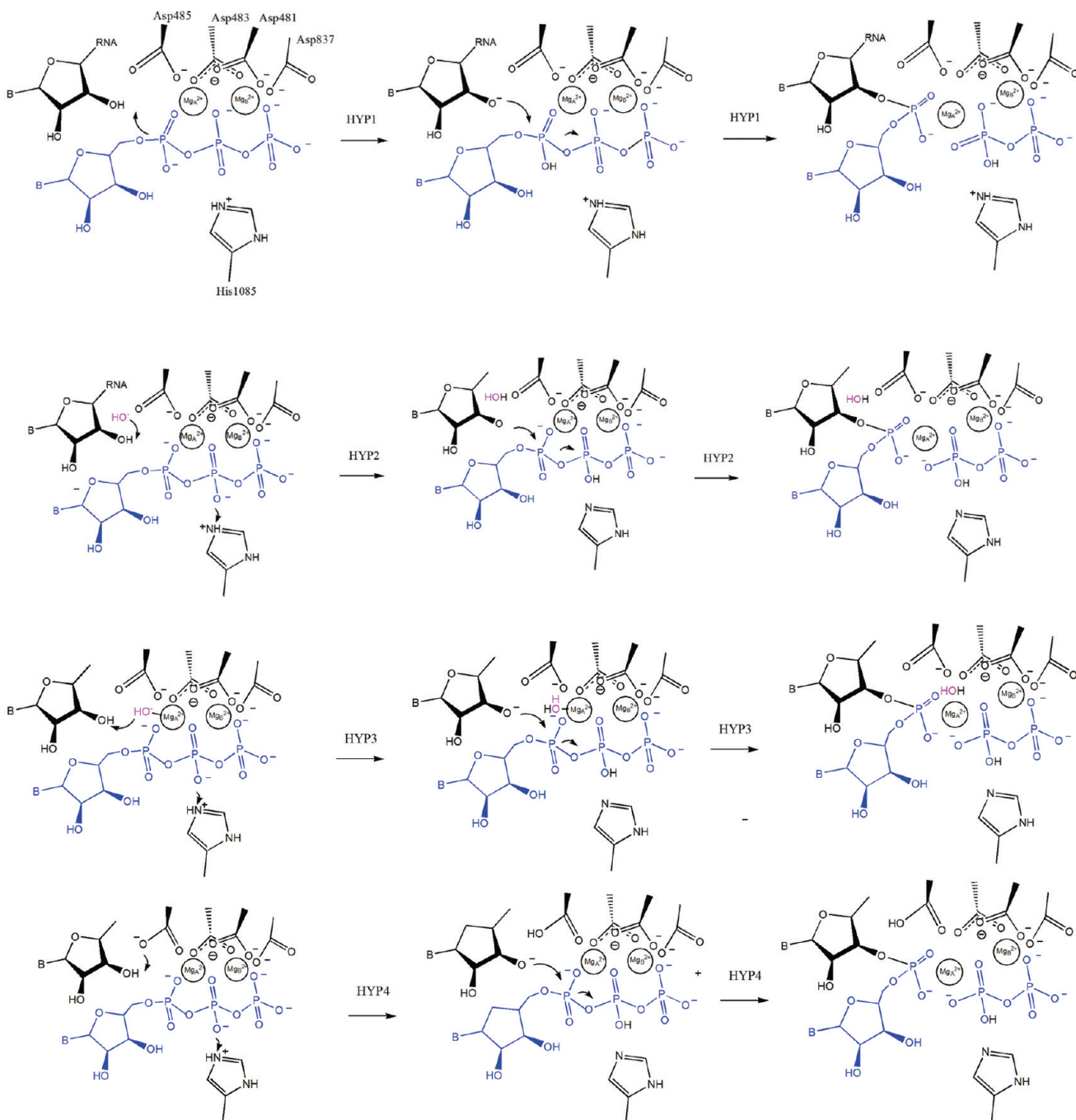
2. METHODOLOGY

2.1. Molecular Dynamics. The molecular dynamics simulations were performed with the Groningen Machine for Chemical Simulations, version 4, Gromacs 4, with the amber99 force field [11].

The models were built using the coordinates of the crystallographic structure of RNAP II from *S. cerevisiae* with PDB code 2E2H.¹ This structure is the most recent structure of RNAP II with the substrate at a low Mg^{2+} concentration. The resolution is 3.95 Å, which is far from excellent but is accurate enough for the study conducted here. The missing loops were modeled resorting to the structures 2NVZ and 2E2I.

The full enzyme was first neutralized by adding 83 Na^+ ions and solvated in a cubic box with 181 875 waters (which corresponds to a distance of at least 10 Å besides the protein atoms). The geometry was optimized with 400 steps of steepest descent minimization. All subsequent simulations were carried out in the NTP ensemble with periodic boundary conditions. The Berendsen temperature coupled with velocity rescaling was employed to maintain a constant temperature at 300 K. The pressure was kept constant at 1 atm with a Parrinello–Rahman barostat. Isotropic position scaling was used to maintain the pressure with a relaxation time of 0.5 ps. The particle mesh Ewald (PME) method was employed to compute the electrostatic interactions with a cutoff of 0.8 nm. LINCS constraints were applied to all bonds involving hydrogen. The time step was 0.002 ps. The trajectory was saved every 1 ps. We performed a total of 50 ps of equilibration and 20 ns of a production run.

Scheme 2. Intramolecular Proton Transfer Followed by Nucleophilic Attack (HYP1), the External HO⁻ Hypothesis (HYP2), the Transfer of the HO_{RNA} Proton to an HO⁻ Coordinated to Mg_A²⁺ (HYP3) and the Transfer of the HO_{RNA} Proton to the Conserved Protein Residue Asp485 (HYP4)



2.2. QM Models. The models included all species relevant for the mechanism, i.e., the substrate (GTP); the 3' terminal nucleotide of the bound RNA; the two Mg²⁺ ions; the catalytic triad (Rpb1-Asp481, 483, and 485); the side chain of Asp837 up to the β carbon (which is also in the coordination sphere of Mg_B²⁺); the side chain of His1085 from Rpb1 (which may act as a general acid in the mechanism); and the side chains of Arg446, Arg766, Arg1020, and Lys967 from Rpb2. These latter residues were included because they engage in H bonds with the oxygen atoms of the triphosphate (Figure 1). A HO⁻ ion was also

included when its participation in the catalytic cycle was hypothesized. The models included 226 atoms in total (228 with HO⁻). The total charge of the models was 0 in the cases where the HO⁻ was included and +1 in the remaining.

The calculations were done with Gaussian 03. We have used the ONIOM method to optimize the geometries. We have used a QM/QM methodology with the high level layer treated with DFT and the remaining with PM3MM. In these instances, the charge transfer is accounted for at the lower level of theory. The subtractive ONIOM method has the same limitations of any

other additive hybrid method within this application, which are related to the less accurate description of the lower level region and interactions between layers. These limitations were greatly alleviated in the final energy calculations, which were done with the full system described at a high level (DFT).

The higher level layer contains the triphosphate of the substrate (GTP), the ribose of the RNA, the two magnesium ions, the δ carbon and the two δ oxygens of the four aspartate residues, His1085 (this last in all cases except in the study of HYP1, as the His here does not participate in the reaction), and the HO^- ion.

A recent study¹⁷ has shown that MPWB1K was the most accurate functional for the description of the hydrolysis of phosphodiester bonds. In the same study, it was concluded that the geometries calculated with B3LYP have negligible differences in relation to the MPWB1K geometries. Concerning the energies, B3LYP was shown to overestimate the barriers by 2.94 kcal/mol and overestimate the reaction energies by 2.02 kcal/mol; given such small differences and the precise knowledge of the inaccuracies involved, we opted to use B3LYP, as this functional is much more numerically stable than the ones that explicitly depend on the kinetic energy density. Numeric stability is crucial in facilitating calculations in a system of this size.

The geometries were optimized at the ONIOM (B3LYP/6-31G(d):PM3MM) level. The energies were calculated with the whole model at the DFT level (B3LYP/6-311++G(2d,2p)). This combination of theoretical levels has been shown in the past to provide geometries and energies accurate enough for the purpose in mind.^{18,19} All stationary points were optimized without constraints.

Frequency calculations were carried out, with the resulting number of imaginary frequencies confirming the nature of the stationary points. The zero point energy and the thermal and entropy contributions for the Gibbs free energy were calculated at the same theoretical level. The electrostatic effect of the remaining protein was accounted for using a dielectric continuum (PCM) with a dielectric constant of 4.

Although the active site of the X-ray structure of RNAP II of Wang et al.¹ (with the substrate before the addition) is similar to some of the reported active sites of DNAPs,^{6,9,20} there are some important differences. The most striking is that Mg_A^{2+} is not positioned between HO_{RNA} and the substrate O_ω but instead well above P_α (Figure 1).

2.3. Thermodynamic Integration. We have simulated the transfer of a HO^- ion from bulk solvent to the protein active site. This was done with the thermodynamic integration (TI) technique, through the annihilation of the ion in bulk solvent and creation of the ion in the proper active site place. The process was carried out in two separate stages, neutralization of the atomic charges and annihilation of the van der Waals parameters. Due to the large size of the enzyme, we have used a sphere with a radius of 25 Å, centered in the HO_{RNA} group.

The TI method allows for computation of the free energy difference between two states by gradually transforming the initial state into the final state. The parameter λ represents the state of the system along the transformation (eq 1):

$$\Delta G_{\text{TI}} = \int_0^1 \left\langle \frac{\partial H(\lambda)}{\partial \lambda} \right\rangle_\lambda d\lambda \quad (1)$$

$H(\lambda)$ is the Hamiltonian for state λ . λ equals zero for the initial state and 1 for the final state. The brackets represent an ensemble

average. As the exact calculation of ΔG_{TI} would require an infinite number of ensemble averages for λ , ranging continuously from 0 to 1, the following approximation is employed:

$$\Delta G_{\text{TI}} = \sum_i \left\langle \frac{\partial H(\lambda)}{\partial \lambda} \right\rangle_\lambda \Delta \lambda_i \quad (2)$$

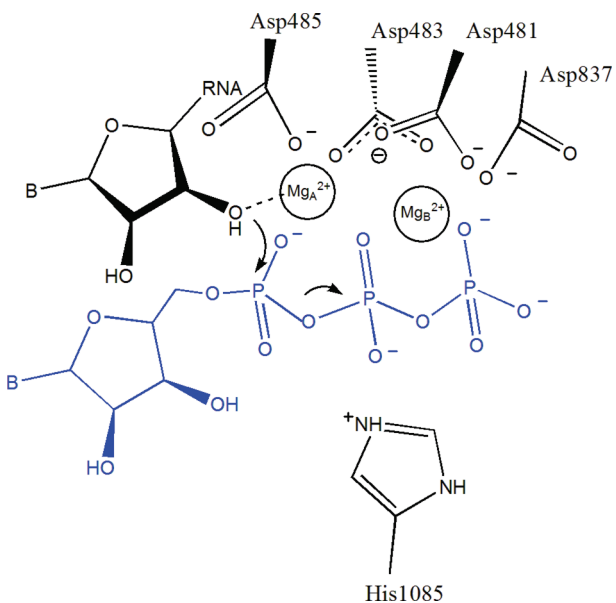
The transformation simulated here (the annihilation of HO^- in aqueous solution and the creation of HO^- in the active site) was performed in two stages with nine λ points each. The first stage, $\lambda = 0.1$, corresponds to the HO^- ion in water (or in the active site), and $\lambda = 0.9$ corresponds to the ion at the same place but without atomic charges (neutralization). In the second stage, we started from the neutral ion ($\lambda = 0.1$) and gradually reduced its van der Waals interactions until $\lambda = 0.9$, where the ion was fully annihilated. At each λ point, we have performed 500 steps of steepest descent minimization, followed by 50 ps of equilibration and 200 ps of a production run. The whole calculation was 4.5 ns-long.

3. RESULTS AND DISCUSSION

Before discussing in detail the mechanistic pathways that we have explored, we will give an overview of the experimental and theoretical backgrounds that made us assume the specific coordination shells of Mg_A^{2+} used here. In the crystallographic structure of RNAP II, Mg_A^{2+} is pentacoordinated and Mg_B^{2+} is tetracoordinated. However, these coordination shells must be interpreted with caution, as the terminal RNA nucleotide misses the HO_{RNA} group (to prevent the attack to the substrate). Therefore, the RNA is necessarily unbound from the Mg_A^{2+} . This is a general limitation present in all crystallographic files of RNAPs and DNAPs. All of those that contain RNA or DNA and the respective substrate must contain a chemical modification to prevent the reaction, usually the deletion of the 3' hydroxyls of the terminal RNA or DNA nucleotides. This modification influences the metal coordination shell. Therefore, it has not been possible to show if many of these enzymes (and specifically RNAP II) indeed have the HO_{RNA} bound to Mg_A^{2+} at the beginning of the cycle.

Several experimental and computational studies give support for a coordination number for Mg^{2+} in the range of four to six.²¹ In aqueous solutions, Mg^{2+} was almost always observed hexacoordinated. In 1999, gas phase electrospray ionization experiments revealed two different $[\text{Mg}(\text{H}_2\text{O})_6]^{2+}$ isomeric forms.²² DFT calculations have shown that in one of these forms Mg^{2+} had a pentacoordinated structure, with the sixth water molecule in the second coordination shell. Pentacoordinated catalytic Mg^{2+} ions were also observed in the X-ray structures of Mg^{2+} containing enzymes such as the Klenow fragment of DNA polymerase I,¹³ the ε subunit of *E. coli* DNA polymerase,²³ the SRP GTPase Ffh,²⁴ ribonuclease H,²⁵ and tryptophanyl-tRNA synthetase.²⁶

In a DFT study on the influence of the identity of the ligands on the coordination number of Mg^{2+} , Kluge and Weston found that the presence of one hydroxide ligand triggers a change from the typically observed octahedral geometry to a trigonal bipyramidal geometry (with five ligands).²⁷ When two hydroxide ions are present, the tetrahedral coordination geometry is preferred. However water, carboxylate, or ammonia ligands were not able to change the preference of Mg^{2+} for the octahedral geometry. Kluge and Weston pointed out that the reason for this preference is electrostatic. However they were unable to find out the actual reasons why HO^- stabilizes the pentacoordinated geometry.

Scheme 3. The CHECK Model

Consequently, other highly charged ligands such as the triphosphate of GTP may also induce a pentacoordinated geometry.

We have performed MD simulations on complexes of RNAP II with RNA/DNA and the substrate in explicit solvent. We have performed three MD runs, two of them without any constraint (besides the bond lengths involving hydrogen atoms). In both of these runs, the relative positions of the magnesium ions have not changed in relation to the X-ray structure: Mg_A^{2+} is maintained close to the oxygens of P_ω and Mg_B^{2+} is kept between P_β and P_γ oxygens.

In the third run, we constrained the position of specific atoms to obtain the configuration that is considered to be more typical for two metal ion catalysis in other enzymes: (i) The distance between the RNA terminus and the Mg_A^{2+} was constrained to 2 Å. (ii) The distance between the two metal ions was kept at 4 Å. (iii) We placed one Mg^{2+} on each side of oxygen 1 α (oxygen of the sicille phosphorus).

We ran the constrained simulation for 1 ns. Afterward, we released the constraints and ran the simulation for an additional 20 ns. When we released the constraints, the atoms changed almost immediately to positions very similar to the ones in the simulations without constraints.

One of the possible explanations for the particular cofactor arrangement in this enzyme is that the active site contains four negative Asp residues (not three Asp/Glu as in DNA polymerases). The position of the Mg^{2+} ions in the two-metal-ion catalysis scheme would create a charge imbalance at P_γ , due to the additional Asp present in RNAP (please see Scheme 1B). For that reason, it can be easily understood that the Mg^{2+} ions adopt the positions reported in Scheme 1A in all simulations.

After making conclusions about the positions of the Mg^{2+} ions, we then wanted to check the position of the HO_{RNA} in relation to Mg_A^{2+} since this was not clear from the MD simulations. In some simulations, the HO_{RNA} was strongly coordinated to Mg_A^{2+} and in others was weakly coordinated. We started the DFT study with a structure in which the HO_{RNA} was in the first coordination shell of Mg_A^{2+} (i.e., strongly coordinated—CHECK model; see Scheme 3). Such a model is

apparently more consistent with the two metal ion catalysis scheme, in which Mg_A^{2+} orients and activates the nucleophile by lowering its pK_a , facilitating the subsequent deprotonation.^{14,15} The closer the HO_{RNA} is to Mg_A^{2+} , the more easily this group will be deprotonated because the Mg_A^{2+} provides a greater stabilization to the product O^-_{RNA} . However, in the subsequent step of that mechanism, this very stable anionic product must unbind from Mg_A^{2+} to attack the substrate, and it is far from obvious that the energetic price for this step would be smaller than the advantage gained in the previous one.

In our DFT calculations, all attempts to attack the substrate starting from a structure with the HO_{RNA} strongly coordinated to Mg_A^{2+} have been unsuccessful. There is no stationary point with the HO_{RNA} deprotonated and bound to Mg_A^{2+} and its proton bound to any of the bases close by (Asp486 or O_α). Transfer of the proton to these bases leads to nonstationary points with energies of 17.0 and 16.8 kcal/mol above the unbound form. Moreover, the movement of the HO_{RNA} toward the substrate P_α causes the unbinding of the HO_{RNA} from Mg_A^{2+} , with a simultaneous decrease in energy, up to a minimum (stationary state) very similar to our DFT model structures in which the HO_{RNA} is weakly coordinated to Mg_A^{2+} . Therefore, the model rearranges and converts spontaneously into the weakly coordinated model, during the movement of the magnesium-bound HO_{RNA} toward the P_α (for nucleophilic attack).

We concluded that the structure with the HO_{RNA} bound to Mg_A^{2+} was outside the catalytic pathway, and therefore we concentrated subsequently on the structures that start with the HO_{RNA} weakly coordinated to Mg_A^{2+} . These will be discussed in detail.

The most straightforward hypothesis (HYP1, Scheme 2) is a proton transfer from HO_{RNA} to O_α . In this case, the deprotonation of the attacking nucleophile and protonation of the leaving group is achieved without the intervention of any additional group. The other three studied pathways (Scheme 2) correspond to the external HO^- hypothesis (HYP2), the transfer of the HO_{RNA} proton to an HO^- coordinated to Mg_A^{2+} (HYP3), and the transfer of the HO_{RNA} proton to the conserved protein residue Asp485 (HYP4). In all of these last three hypotheses, we found that protonation of the leaving group could be achieved by His1085. The external HO^- hypothesis resulted in the most feasible mechanism for RNAP II.

3.1. Intramolecular Proton Transfer Followed by Nucleophilic Attack (HYP1). This hypothesis of a mechanism begins with the transfer of the HO_{RNA} proton to the O_α atom. We have started with this case because it includes the two proton transfer reactions in a very straightforward way. The substrate O_α would act first as a base, deprotonating HO_{RNA} , and then act as an acid, protonating the leaving PPi (substrate assisted catalysis). We have also tested the influence of the basis set used in the calculations in this specific reaction pathway.

The direct transfer of the HO_{RNA} proton to the O_α atom from the reactants (R) does not lead to a stationary point (the protonated O_α atom lies 25.1 kcal/mol above the reactants, Figure 2). However, upon rearrangement of the $H-O_{1\alpha}-P_\alpha-O_S$ dihedral (such that this group engages in a hydrogen bond with an O_γ atom), we found a stationary state with the proton transferred to the O_α atom (structure I_{dRNA} in Figure 2). I_{dRNA} lies 24.9 kcal/mol above the initial reactants. The distance between ion O^-_{RNA} and atom P_α is 3.36 Å, and the distance between atom P_α and the ether oxygen atom of the scissile bond ($O_{3\beta}$) is 1.62 Å. We have not located the transition

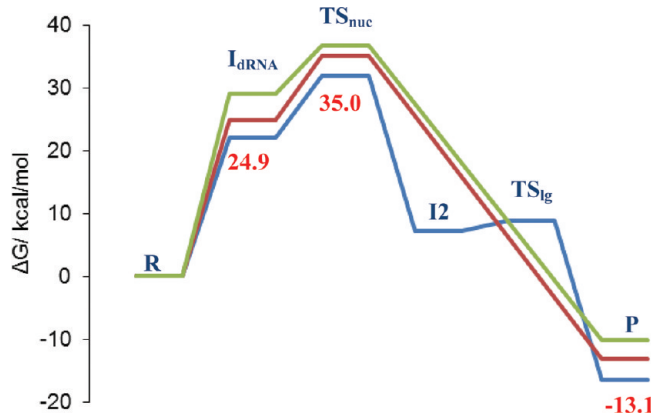


Figure 2. Potential energy surfaces for the HYP1 pathway calculated with different basis sets. Blue, B3LYP/6-31G(d)//ONIOM(B3LYP/6-31G(d):PM3MM); red, B3LYP/6-311++G(2d,2p)//ONIOM(B3LYP/6-31G(d):PM3MM); green, B3LYP/6-311++G(2d,2p)//ONIOM(B3LYP/6-311++G(2d,2p):PM3MM). As can be seen, the shape of the PES is the same whenever the optimization is done with the smaller or larger basis sets, as long as the final energies are calculated with the larger basis sets.

state between R and I_{dRNA} because the energy barrier for the subsequent steps of this pathway is too high to match the enzyme kinetics, as will be seen below. The transition state for the nucleophilic attack of ion O^-_{RNA} to the P_α atom (TS_{nuc} , Figure 3) is directly connected to I_{dRNA} and has an energy of 10.1 kcal/mol above that of the reactants (Figure 2). The bond between ion O^-_{RNA} and the P_α atom is being formed (2.14 Å), and the bond between the P_α and the $O_{3\beta}$ atoms is starting to break (1.73 Å). Decay from TS_{nuc} leads to structure I_2 , a pentacoordinated intermediate. In this structure, the $O^-_{RNA} \cdots P_\alpha$ distance is 1.75 Å and the $P_\alpha \cdots O_{3\beta}$ distance is 1.80 Å. I_2 is 13.1 kcal/mol above R. Elimination of PPi (the leaving group, lg) proceeds through a second transition state TS_{lg} 11.5 kcal/mol above R. In TS_{lg} (Figure 3), the $O_{3\beta}$ atom is moving away from the P_α atom and starting to form a bond with the proton of the O_α atom. The $O^-_{RNA} \cdots P_\alpha$ distance is now 1.65 Å, and the $P_\alpha \cdots O_{3\beta}$ distance is 2.48 Å. Finally, the products (P) correspond to the protonated PPi and the substrate incorporated in the RNA chain. The products are 13.1 kcal/mol below R. The new phosphodiester bond ($O^-_{RNA} \cdots P_\alpha$) has a bond length of 1.65 Å, and the $O_{3\beta}$ atom of PPi has moved 3.40 Å away from the P_α atom. Figure 3 shows a detail of the two transition states discussed in the text. To complete the catalytic cycle, the PPi must subsequently leave the active site, and RNA must translocate one base pair away from the active site. The reaction is exoenergetic, as expected, as we are breaking a highly energetic bond (Figures 2 and 3). The energy barrier between the reactants (R) and the highest point along the pathway (TS_{nuc}) amounts to 34.9 kcal/mol, which is clearly too high for an enzymatic reaction. The turnover number for the enzyme is 0.16 s^{-1} , from which a rate-limiting barrier of 18.1 kcal/mol can be derived. Consequently, regardless of whether the rate limiting step of the reaction is the conformational transition (trigger loop closing) or the chemical step, any of the associated barriers must lie below (or be equal to) 18.1 kcal/mol.

When dealing with negatively charged systems (such as this one), the use of diffuse functions is highly recommended. To be on the safe side we decided to reoptimize the structures using a

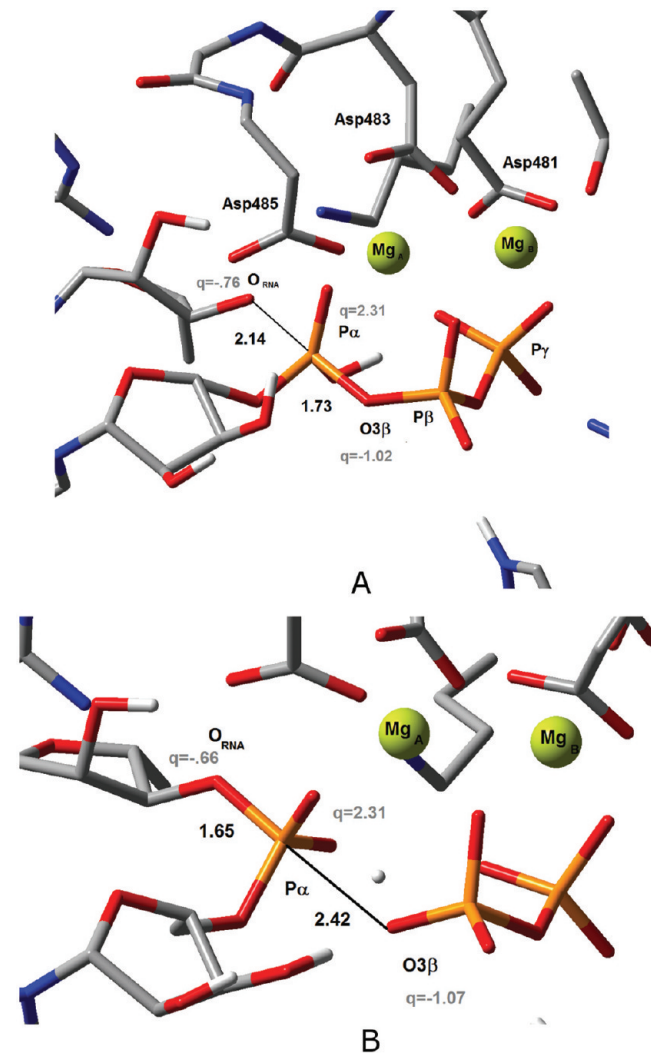


Figure 3. A detailed illustration of the structures of TS_{nuc} and TS_{lg} for HYP1. TS_{nuc} (A) is the transition state related with the nucleophilic attack of O^-_{RNA} to P_α . TS_{lg} (bottom) is the transition state associated with proton transfer to PPi and elimination of the PPi from the pentacoordinated complex. Relevant distances and Mulliken atomic charges q are shown.

triple- ζ basis set with diffuse functions and extra polarization functions, namely, 6-311G++(2d,2p) (Figure 2). A comparison of the three energy profiles shows that the B3LYP/6-311G++(2d,2p)//B3LYP/6-31G(d) curve represents a good compromise between PES accuracy and computational time. The smaller basis set identifies the pentacoordinated species as a transient short-lived intermediate. When the PES is calculated at the B3LYP/6-311G++(2d,2p)//B3LYP/6-31G(d) level, the energy of the second transition state becomes lower than that of the pentacoordinated intermediate, giving rise to a profile equivalent to the B3LYP/6-311G++(2d,2p)//B3LYP/6-311G++(2d,2p) PES.

As the activation and reaction energies obtained for the nucleophilic attack with this computational methodology were small (10.1 kcal/mol at the B3LYP/6-311G++(2d,2p)//B3LYP/6-31G(d) level), we were motivated to search for alternative residues that could deprotonate the HO^-_{RNA} more efficiently, eliminating the high barriers associated with this step.

3.2. The External HO⁻ Group hypothesis (HYP2). This hypothesis assumes that the proton of the HO_{RNA} group is abstracted by a HO⁻ ion coming from bulk solution. Therefore, one of the protein residues must protonate the PPi. The only residue that is appropriately positioned and has the adequate acidic character near the triphosphate of the substrate is His1085. In the reactants (R), we have included a HO⁻ ion establishing hydrogen bonds with both the 2'HO and the 3'HO of the RNA terminus. This position was chosen because it is the only stationary point we could find close enough from the HO_{RNA} group for an efficient deprotonation.

To measure the energy involved in transferring a HO⁻ ion from the bulk solvent to the active site, we needed to calculate the free energy of transfer and correct it for the nonstandard state associated with the low concentration of the ion at physiological pH. A preliminary search for the most stable and catalytic competent positions for the HO⁻ ion showed us that the correct place for the HO⁻ ion was doubly hydrogen bonded to both the hydroxyl groups of the terminal RNA, between them and the Mg²⁺ ion. This position is the most stable one that obeys the requisite of having the hydroxyl ion hydrogen bonded to the HO_{RNA} that will be deprotonated.

The free energy of transfer between the two media (bulk solvent and active site) was accounted for by a classical molecular dynamics thermodynamic integration and resulted in -4.20 ± 0.52 kcal/mol. The gain in water–water interactions and the strong interactions between the ion and the terminal RNA make this step favorable. However, in reality, the ion is present in the system at a much lower concentration of 10^{-7} mol·dm⁻³. The translational entropy lost in the confinement of the ion from its volume in bulk solution to a volume of 1–3 water molecules (the volume in which it can move without disturbing the two hydrogen bonds) is known to be 12.4–11.7 kcal/mol, respectively. This value is not very sensitive to the exact volume of confinement. Taking the volume of three water molecules as a reference, we end up with a cost of +7.5 kcal/mol for bringing a HO⁻ ion from bulk solution to the active site, hydrogen bonded to the HO_{RNA} group and ready for deprotonation.

In R, the hydrogen bonds have a length of 1.90 Å and 1.62 Å from the 2'HO and 3'HO (i.e., HO_{RNA}) groups. The distance between the HO_{RNA} group and the P_α atom is 3.48 Å. The barrier for deprotonation is so shallow that we were not able to optimize it. Each time we tried, the system decayed to I_{dRNA}, in which the HO_{RNA} proton is transferred to the HO⁻ group and the hydrogen bond with the 2'HO is broken. The distance between the O⁻_{RNA} ion and the new water molecule is 1.54 Å. The O⁻_{RNA} ion is now at 3.37 Å from the P_α atom. I_{dRNA} lies 4.9 kcal/mol below R. The proton transfer is energetically favorable (Figure 5). In the second step, the ε2 proton from the positively charged His1085 (H_{ϵ}^+) is transferred to the O_{1β} atom of the triphosphate through the transition state TS_{lg} (Figure 4). The distance between the proton H_ε⁺ and the O_{1β} atom is 1.43 Å, and the His1085 N_ε···H_ε⁺ distance is 1.16 Å. The reaction barrier for this proton transfer is 7.2 kcal/mol. The order of the two proton transfers may be interchanged; i.e., the protonation of PPi may occur prior to deprotonation of the HO_{RNA} group. This will depend on the kinetics of diffusion of the HO⁻ ion into the active site. After the proton transfer (structure I_{lg}), the distance between O⁻_{RNA} and P_α is 3.06 Å. Subsequently, O⁻_{RNA} attacks P_α via a pentacovalent transition state (TS_{nuc}) with an associated reaction barrier of 9.1 kcal/mol (Figure 4). In TS_{nuc}, the distance between O⁻_{RNA} and P_α is 2.17 Å, and the distance between the P_α and O_{3β} atoms increases to 1.73 Å in HYP1 and 1.92 Å in HYP2. Finally, in the product (P), the distance between the P_α and O_{3β} atoms increases to 3.70 Å, and the bond between P_α and O⁻_{RNA} is fully formed (1.68 Å). The product is 15.7 kcal/mol below TS_{nuc} and 13.3 kcal/mol below R, as expected, since we are breaking a highly energetic phosphodiester bond (Figure 5).

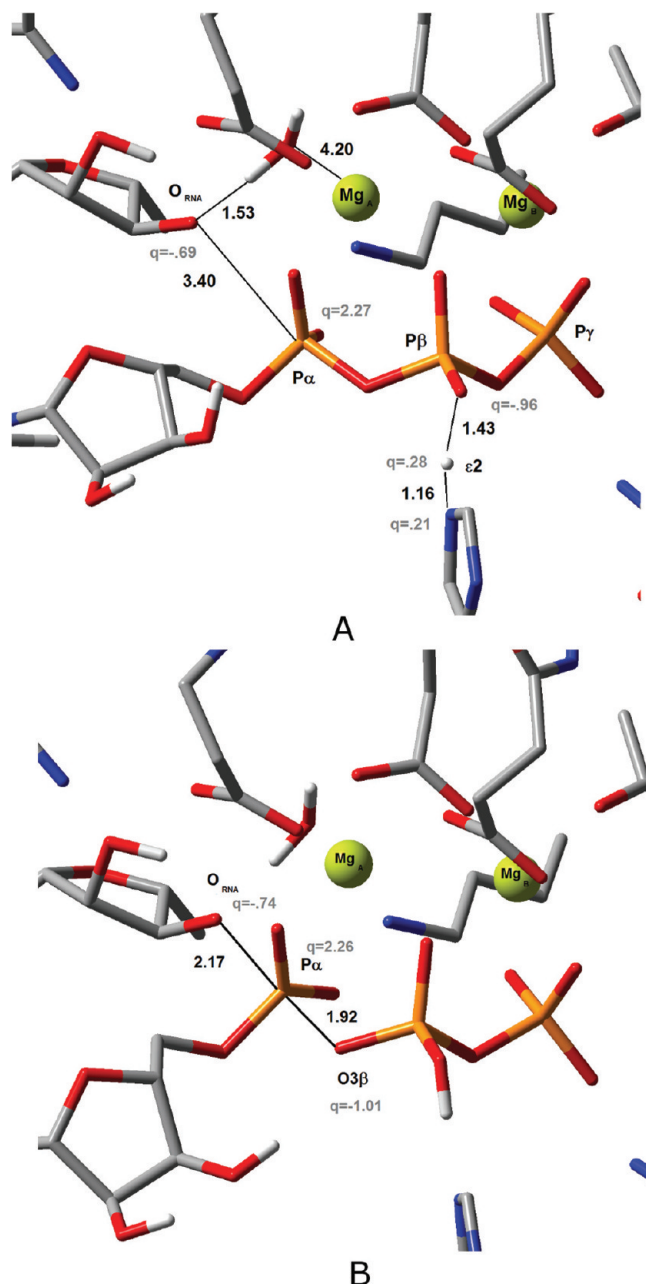


Figure 4. Structures of the transition states for hypothesis HYP2. TS_{lg} (top) is the transition state related with the proton transfer between His1085 and the O_β atom of the substrate triphosphate. TS_{nuc} (bottom) is the transition state associated with the nucleophilic attack of O⁻_{RNA} to P_α. Relevant distances and Mulliken atomic charges *q* are shown.

P_α and O_{3β} atoms amounts to 1.92 Å. This TS is very similar to the one for nucleophilic attack in HYP1. The energy of TS_{nuc} in relation to its reactants is 9.1 kcal/mol compared with the 10.5 kcal/mol of HYP1. The distance between O⁻_{RNA} and P_α is 2.14 Å in HYP1 and 2.17 in HYP2, and the distance between the P_α and O_{3β} atoms amounts to 1.73 Å in HYP1 and 1.92 Å in HYP2. Finally, in the product (P), the distance between the P_α and O⁻_{RNA} is fully formed (1.68 Å). The product is 15.7 kcal/mol below TS_{nuc} and 13.3 kcal/mol below R, as expected, since we are breaking a highly energetic phosphodiester bond (Figure 5).

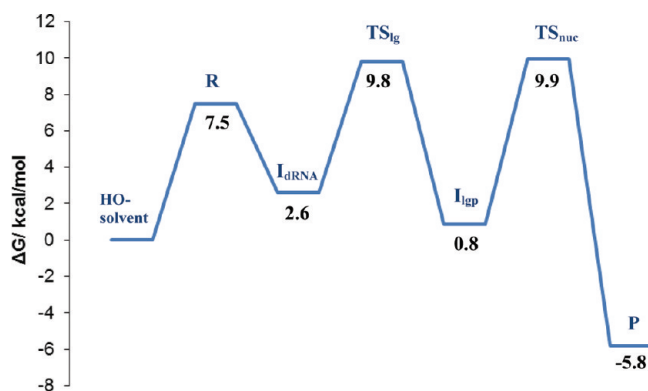


Figure 5. Potential energy surface for the mechanistic hypothesis HYP2. We have estimated that the transfer of the HO^- from the bulk solvent to the active site requires 7.5 kcal/mol. The proton transfer from His1085 (TS_{ig}) to the substrate triphosphate was a free energy barrier of 7.2 kcal/mol, and the nucleophilic attack (TS_{nuc}) was a free energy barrier of 9.1 kcal/mol. The products lie 13.3 kcal/mol below the reactants and 5.8 kcal/mol below the state with the hydroxyl in solution.

In total, starting from the hydroxyl ion in solution, the rate-limiting free energy barrier (the nucleophilic attack) amounts to 9.9 kcal/mol, and the reaction free energy corresponds to -5.8 kcal/mol.

3.3. Deprotonation by a HO^- Bound to Mg_A^{2+} and Protonation by His1085. A third hypothesis (HYP3) involves an initial proton transfer from the HO_{RNA} to a hydroxide ion bound to Mg_A^{2+} (instead of a free HO^- ion coming from the bulk solution) and the transfer of a proton from Hist1085 to PP*i*, followed by nucleophilic attack. Even though the X-ray structure does not show such an ion coordinated to Mg_A^{2+} , this hypothesis shall not be excluded, as (i) the reduced water content of the structure can cause an impact on the existence of such ions and (ii) this hypothesis might correspond to an extension of the previous, in which the hydroxyl ion diffuses from the bulk solution and subsequently binds Mg_A^{2+} afterward. The difference here is that the ion would bind the Mg_A^{2+} before deprotonating the HO_{RNA} group.

The modeling of the HO^- ion in the coordination sphere of Mg_A^{2+} led to significant rearrangements. The $\text{O}_{2\beta}$ atom unbound from the Mg_A^{2+} cation, and the latter changed to a tetrahedral coordination geometry, getting closer to the HO_{RNA} group and away from Mg_A^{2+} .

The HO^- ion is now much closer to the substrate than in HYP2. Its negative charge polarizes further the substrate and increases the pK_a of the $\text{O}_{1\beta}$ atom, which spontaneously abstracts a proton from His1085.

In the reactants (R_{lg}), the distance between the Mg^{2+} ions is 4.93 Å, the distance between the HO_{RNA} and Mg_A^{2+} is 3.67 Å, and the distance between Mg_A^{2+} and $\text{O}_{2\beta}$ is 4.14 Å. The 2'HO and 3'HO (HO_{RNA}) groups of the terminal RNA nucleotide both establish hydrogen bonds with the magnesium-bound HO^- ion, with distances of 1.72 Å and 1.61 Å. The distance between the HO_{RNA} and P_α is 3.60 Å. The distance between HO^- and Mg_A^{2+} is 1.95 Å.

To see if the binding of HO^- to Mg_A^{2+} (HYP3) is thermodynamically favored over the weak interaction of the ion with the metal (HYP2), we disconnected the hydroxide from Mg_A^{2+} and reoptimized the structure, generating the reactants of HYP2. The energy dropped by 10.8 kcal/mol, showing that the structure of

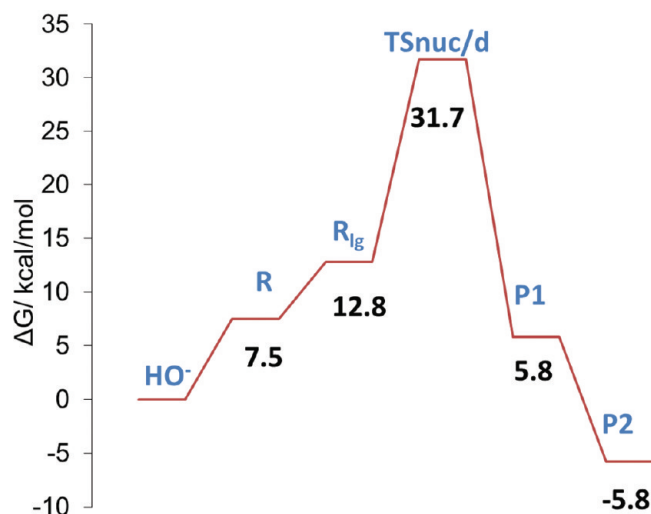
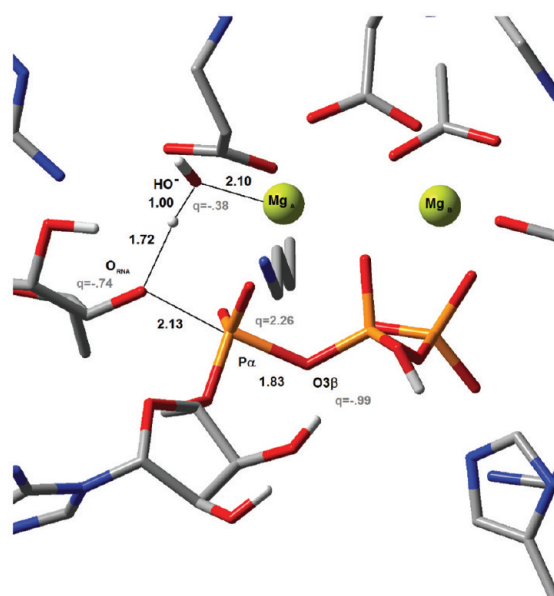


Figure 6. (Top) Structure of the transition state for HYP3 ($\text{TS}_{\text{nuc}/\text{dRNA}}$). The transition state is related to the nucleophilic attack of P_α by O_{RNA}^- and the proton transfer from the HO_{RNA} group to the HO^- ion. Relevant distances and Mulliken atomic charges q are shown. (Bottom) Free energy profile for HYP3. The energy barrier for $\text{TS}_{\text{nuc}/\text{dRNA}}$ is 18.9 kcal/mol.

HYP2 (HO^- near but unbound from Mg_A^{2+}) is preferred. Anyway, the binding of HO^- to Mg_A^{2+} could lower the rate-limiting barrier for the reaction and bring an overall benefit in terms of the kinetics of the transformation. Therefore, we continued to follow this mechanism.

The transition state ($\text{TS}_{\text{nuc}/\text{dRNA}}$) corresponds to the nucleophilic attack on the P_α atom, concerted with the transfer of the proton of the HO_{RNA} group to the metal bound HO^- ion (Figure 6). In this structure, the distance between the HO_{RNA} and P_α groups shortens to 2.13 Å, and the distance between the P_α and $\text{O}_{3\beta}$ atoms increases to 1.83 Å. The distance between the Mg_A^{2+} ion and the $\text{O}_{2\beta}$ atom changes to 2.28 Å, and Mg_A^{2+} becomes pentacoordinated again. The two Mg^{2+} ions approach

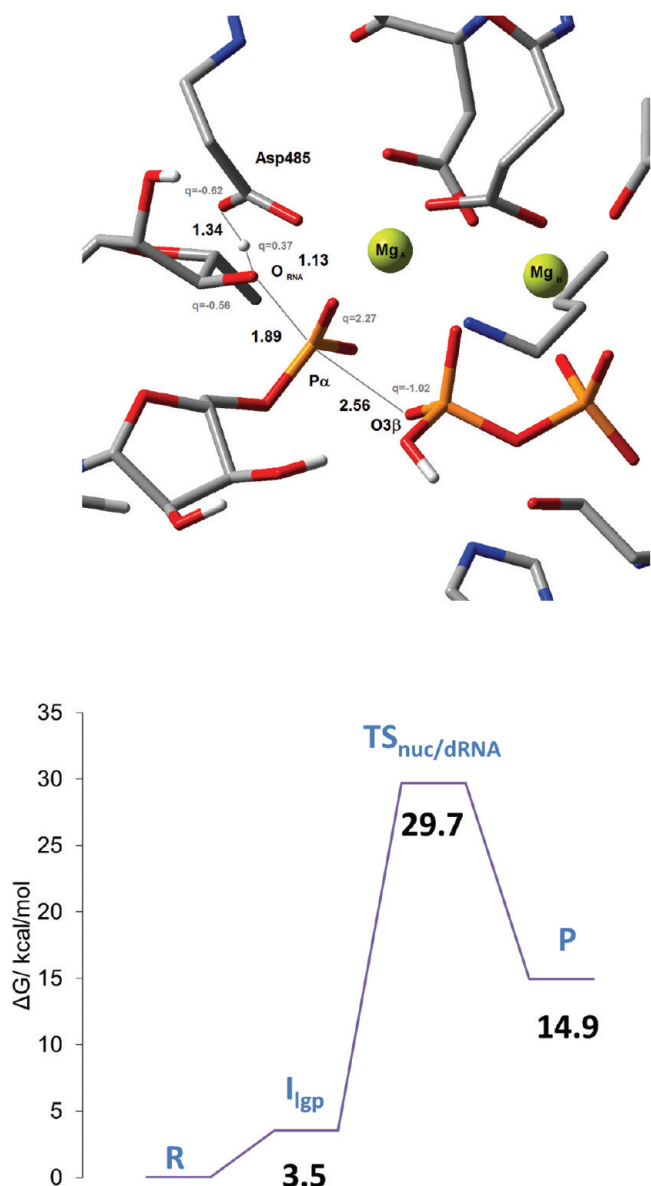


Figure 7. Structure of the transition state. The transition state is related with nucleophilic attack of HO_{RNA} to P_α and simultaneous proton transfer from the HO_{RNA} to Asp485 ($\text{TS}_{\text{nuc/dRNA}}$). Relevant distances and Mulliken atomic charges are shown. (Bottom) Free energy profile for HYP4. The free energy barrier for $\text{TS}_{\text{nuc/dRNA}}$ is 26.2 kcal/mol.

3.76 Å, which is closer to the values observed in HYP1 and HYP2. The energy barrier for this step is 18.9 kcal/mol. In this case, the nucleophilic attack is kinetically much less favorable than in HYP2 (Figure 6). In the products, the $\text{O}_{3\beta}$ atom separates from P_α (2.98 Å). The difference in energy between P and the reactants is −6.9 kcal/mol.

Comparing the final structures of HYP2 and HYP3, we can see that the difference lies in the coordination of the water molecule to Mg^{2+} , which is clearly unfavorable. Upon dissociation of the water molecule, the energy of the system drops by 11.6 kcal/mol, and the final reaction energy is −18.6 kcal/mol.

Starting from the initial system with the hydroxide in solution, the barrier amounts to 31.7 kcal/mol and the reaction energy to −5.8 kcal/mol.

Table 1. Reaction Steps for Each Hypothesis^a

	reaction steps
HYP1	1 proton transfer from HO_{RNA} to O_α 2 nucleophilic attack (O_{RNA}^- on P_α)
HYP2	1 HO^- transfer to active site 2 proton transfer HO_{RNA} to HO^- 3 proton transfer from His1085 to O_β 4 nucleophilic attack
HYP3	1 HO^- transfer from bulk solvent to the active site 2 proton transfer from His1085 to O_β 3 nucleophilic attack and proton transfer from HO_{RNA} to HO^- 4 dissociation of H_2O from Mg_A^{2+}
HYP4	1 proton transfer from His1085 to O_β 2 nucleophilic attack and proton transfer HO_{RNA} to Asp485

^a The CHECK hypothesis was not included because it does not lead to stationary points or it converts into other models already considered in the four hypotheses on the table.

3.4. Transfer of the Proton to Asp485 Concerted with Nucleophilic Attack. The last hypothesis (HYP4), frequently pointed out for DNA polymerases, is a proton transfer from the HO_{RNA} group to a conserved aspartate at the active site. In RNAP II, the only residue in position to fulfill this role is Asp485. However, when we tried to transfer the proton prior to the nucleophilic attack, our calculations have shown that the product of the proton transfer was not a stationary point in the potential energy surface and laid 33.6 kcal/mol above the reactants. Therefore, we tried a case in which the proton transfer from the HO_{RNA} group to Asp485 occurred simultaneously with the nucleophilic attack of the O_{RNA}^- ion to the P_α atom (Figure 7). In the initial reactants (R), His1085 is protonated and the HO_{RNA} group is at 3.54 Å from the P_α . In I_{lgp} , the proton is already in the triphosphate; the HO_{RNA} group is almost at the same distance from the P_α atom (3.57 Å). This structure is 3.5 kcal/mol above R. The structure is thus ready for the subsequent nucleophilic attack. From here, we found the transition state for that reaction ($\text{TS}_{\text{nuc/dRNA}}$), which in fact corresponded to the nucleophilic attack concerted with the proton transfer to Asp485. The $\text{HO}_{\text{RNA}} \cdots \text{HO}$ bond is elongated to 1.13 Å, and the distance between the HO_{RNA} proton and the Asp485 O_γ corresponds to 1.34 Å. The O_{RNA}^- ion approached the P_α atom up to 1.89 Å, and the $\text{P}_\alpha \cdots \text{O}_{3\beta}$ distance elongated to 2.56 Å. The Mg_A^{2+} and Mg_B^{2+} ions came closer to each other (3.20 Å). The activation free energy for this step amounted to 26.2 kcal/mol (Figure 7). In the products (P), the bond between the P_α and the O_β atoms got broken (2.95 Å), and the new phosphodiester bond ($\text{O}_{\text{RNA}}^- \text{P}_\alpha$) was formed (1.66 Å). The products' energies were 14.5 kcal/mol more than that of the reactants. The high activation energy excludes this hypothesis, as the pathway studied in HYP2 is kinetically much more favorable.

4. CONCLUSIONS

Multisubunit RNAPs are evolutionarily unrelated with both single RNAPs and DNAPs. Nevertheless, they catalyze the same

chemical reaction, the polymerization of nucleotides into a nucleic acid chain. The X-ray structures of RNAPII¹ have the Mg_A²⁺ ion in a different position than the one observed for some DNAPs, not located between the HO_{RNA} and P_α groups but instead above the P_α atom.

In the X-ray structures of polymerases with nucleic acid chains and the substrate, the nucleophile (the HO_{RNA/DNA}) is absent to prevent the conversion of the substrate into the exoenergetic product. Consequently, the arrangement of the HO_{RNA/DNA} in relation to the Mg_A²⁺ ion cannot be determined from the X-ray structures. The two-metal-ion scheme hypothesizes that the HO_{RNA} group should be coordinated to the Mg_A²⁺ ion at the beginning of the catalytic cycle. However, our DFT results strongly suggest that such a structure is less stable than a second one with the HO_{RNA} just weakly coordinated to the metal. This result is consistent with a molecular dynamics study of DNA polymerase β in which the coordination distance reported between the HO_{DNA} group and the Mg_A²⁺ ion in the reactant structure was 4.7 Å.²⁸ Moreover, if we start from a HO_{RNA} group strongly coordinated to the Mg_A²⁺ ion, the catalytic pathway necessarily evolves through a HO_{RNA}–Mg_A²⁺ unbinding before the proton transfers and the nucleophilic attack. The structure of the active site does not allow for a nucleophilic attack without a prior HO_{RNA}–Mg_A²⁺ dissociation. Further studies are needed to elucidate if the enzyme has the HO_{RNA} group bound to the Mg_A²⁺ ion before the catalytic cycle begins. However, what we can clearly conclude is that if such state exists it will represent only a precatalytic state and the dissociation of the HO_{RNA} group is a necessary condition for the catalytic reaction to begin.

We have studied the four possible hypotheses for the catalytic pathway. They mostly account for different participants in the acid/base catalyzed proton transfer reactions (deprotonation of HO_{RNA} and protonation of PPi) (Table 1). A comparison of the thermodynamic and kinetic profiles of the four pathways clearly shows that the one described in HYP2 (the external HO⁻ group hypothesis) is by far the most favorable. This pathway involves deprotonation of the HO_{RNA} group by a bulk solvent hydroxide ion, protonation of PPi by His1085, and nucleophilic attack of the triphosphate by the O⁻_{RNA} ion. The rate-limiting step is the nucleophilic attack with an energy barrier of 9.9 kcal/mol relative to the initial state.

Our mechanism for RNAP II differs from the mechanisms proposed for DNAPs in the position of the HO_{RNA} nucleophile in relation to the Mg_A²⁺ ion. It also differs in the protonation of the leaving pyrophosphate, because we have taken into consideration the most recent findings by Castro et al. (role of His1085).^{2,3} The mechanism is consistent with the mechanisms of DNAPs by Flórian et al.^{10,29,30} in regard to the acceptors of the HO_{RNA/DNA} proton. The mechanism is consistent with the mechanisms for DNAPs by Alberts et al.²⁰ and Lin et al.⁵ in regard to the nature of the nucleophilic transition state. We found a single transition state associated with the nucleophilic attack with an O⁻_{RNA}···P_α distance of 2.17 Å (which compares to 2.20 in ref 5) and a P_α···O_{3β} distance of 1.92 Å (which compares to 1.90 in ref 5). Only one TS associated with the nucleophilic attack was found in both works.

ASSOCIATED CONTENT

Supporting Information. RMSDs for the α carbons. This material is available free of charge via the Internet at <http://pubs.acs.org>.

AUTHOR INFORMATION

Corresponding Author

*E-mail: mjramos@fc.up.pt

ACKNOWLEDGMENT

The authors thank the FCT—Fundação para a Ciência e Tecnologia—for financial support.

REFERENCES

- Wang, D.; Bushnell, D. A.; Westover, K. D.; Kaplan, C. D.; Kornberg, R. D. Structural basis of transcription: role of the trigger loop in substrate specificity and catalysis. *Cell* **2006**, *127*, 941–54.
- Castro, C.; Smidansky, E.; Maksimchuk, K. R.; Arnold, J. J.; Korneeva, V. S.; Gotte, M.; Konigsberg, W.; Cameron, C. E. Two proton transfers in the transition state for nucleotidyl transfer catalyzed by RNA- and DNA-dependent RNA and DNA polymerases. *Proc. Natl. Acad. Sci. U.S.A.* **2007**, *104*, 4267–4272.
- Castro, C.; Smidansky, E. D.; Arnold, J. J.; Maksimchuk, K. R.; Moustafa, I.; Uchida, A.; Gotte, M.; Konigsberg, W.; Cameron, C. E. Nucleic acid polymerases use a general acid for nucleotidyl transfer. *Nat. Struct. Mol. Biol.* **2009**, *16*, 212–218.
- Rittenhouse, R. C.; Apostoluk, W. K.; Miller, J. H.; Straatsma, T. P. Characterization of the active site of DNA polymerase beta by molecular dynamics and quantum chemical calculation. *Proteins* **2003**, *53*, 667–82.
- Lin, P.; Pedersen, L. C.; Batra, V. K.; Beard, W. A.; Wilson, S. H.; Pedersen, L. G. Energy analysis of chemistry for correct insertion by DNA polymerase beta. *Proc. Natl. Acad. Sci. U. S. A.* **2006**, *103*, 13294–9.
- Flórian, J.; Goodman, M. F.; Warshel, A. Computer simulation of the chemical catalysis of DNA polymerases: Discriminating between alternative nucleotide insertion mechanisms for T7 DNA polymerase. *J. Am. Chem. Soc.* **2003**, *125*, 8163–8177.
- Abashkin, Y. G.; Erickson, J. W.; Burt, S. K. Quantum chemical investigation of enzymatic activity in DNA polymerase beta. A mechanistic study. *J. Phys. Chem. B* **2001**, *105*, 287–292.
- Bojin, M. D.; Schlick, T. A quantum mechanical investigation of possible mechanisms for the nucleotidyl transfer reaction catalyzed by DNA polymerase beta. *J. Phys. Chem. B* **2007**, *111*, 11244–11252.
- Florian, J.; Goodman, M. F.; Warshel, A. Computer simulation studies of the fidelity of DNA polymerases. *Biopolymers* **2003**, *68*, 286–299.
- Florian, J.; Goodman, M. F.; Warshel, A. Computer simulations of protein functions: searching for the molecular origin of the replication fidelity of DNA polymerases. *Proc. Natl. Acad. Sci. U. S. A.* **2005**, *102*, 6819–24.
- Fothergill, M.; Goodman, M. F.; Petruska, J.; Warshel, A. Structure-Energy Analysis of the Role of Metal-Ions in Phosphodiester Bond Hydrolysis by DNA-Polymerase-I. *J. Am. Chem. Soc.* **1995**, *117*, 11619–11627.
- Kaplan, C. D.; Larsson, K. M.; Kornberg, R. D. The RNA polymerase II trigger loop functions in substrate selection and is directly targeted by alpha-amanitin. *Mol. Cell* **2008**, *30*, 547–556.
- Beese, L. S.; Steitz, T. A. Structural Basis for the 3'-5' Exonuclease Activity of Escherichia-Coli DNA-Polymerase-I - a 2 Metal-Ion Mechanism. *EMBO J.* **1991**, *10*, 25–33.
- Steitz, T. A.; Steitz, J. A. A General 2-Metal-Ion Mechanism for Catalytic Rna. *Proc. Natl. Acad. Sci. U.S.A.* **1993**, *90*, 6498–6502.
- Steitz, T. A. Structural biology - A mechanism for all polymerases. *Nature* **1998**, *391*, 231–232.
- Yang, W.; Lee, J. Y.; Nowotny, M. Making and breaking nucleic acids: Two-Mg²⁺-ion catalysis and substrate specificity. *Mol. Cell* **2006**, *22*, 5–13.
- Ribeiro, A. J. M.; Ramos, M. J.; Fernandes, P. A. Benchmarking of DFT Functionals for the Hydrolysis of Phosphodiester Bonds. *J. Chem. Theory Comput.* **2010**, *6*, 2281–2292.

- (18) Noddleman, L.; Lovell, T.; Han, W.-G.; Li, J.; Himo, F. Quantum Chemical Studies of Intermediates and Reaction Pathways in Selected Enzymes and Catalytic Synthetic Systems. *Chem. Rev.* **2004**, *104*, 459–508.
- (19) Leopoldini, M.; Marino, T.; Michelini, M.; Rivalta, I.; Russo, N.; Sicilia, E.; Toscano, M. The role of quantum chemistry in the elucidation of the elementary mechanisms of catalytic processes: from atoms, to surfaces, to enzymes. *Theor. Chem. Acc.* **2007**, *117*, 765–779.
- (20) Alberts, I. L.; Wang, Y.; Schlick, T. DNA polymerase beta catalysis: Are different mechanisms possible? *J. Am. Chem. Soc.* **2007**, *129*, 11100–11110.
- (21) Kluge, S.; Weston, J. Can a hydroxide ligand trigger a change in the coordination number of magnesium ions in biological systems? *Biochemistry* **2005**, *44*, 4877–85.
- (22) Rodriguez-Cruz, S. E.; Jockusch, R. A.; Williams, E. R. Hydration energies and structures of alkaline earth metal ions, $M^{2+}(H_2O)_n$, $n=5–7$, $M = Mg, Ca, Sr$, and Ba . *J. Am. Chem. Soc.* **1999**, *121*, 8898–8906.
- (23) Cisneros, G. A.; Perera, L.; Schaaper, R. M.; Pedersen, L. C.; London, R. E.; Pedersen, L. G.; Darden, T. A. Reaction Mechanism of the epsilon Subunit of E-coli DNA Polymerase III: Insights into Active Site Metal Coordination and Catalytically Significant Residues. *J. Am. Chem. Soc.* **2009**, *131*, 1550–1556.
- (24) Focia, P. J.; Alam, H.; Lu, T.; Ramirez, U. D.; Freymann, D. M. Novel protein and Mg^{2+} configurations in the $Mg(2+)$ GDP complex of the SRP GTPase Ffh. *Protein: Struct. Funct. Genet.* **2004**, *S4*, 222–230.
- (25) Nowotny, M.; Yang, W. Stepwise analyses of metal ions in RNase H catalysis from substrate destabilization to product release. *EMBO J.* **2006**, *25*, 1924–1933.
- (26) Kapustina, M.; Carter, C. W. Computational studies of tryptophanyl-tRNA synthetase: Activation of ATP by induced-fit. *J. Mol. Biol.* **2006**, *362*, 1159–1180.
- (27) Kluge, S.; Weston, J. Can a hydroxide ligand trigger a change in the coordination number of magnesium ions in biological systems? *Biochemistry* **2005**, *44*, 4877–4885.
- (28) Yang, L.; Arora, K.; Beard, W. A.; Wilson, S. H.; Schlick, T. Critical role of magnesium ions in DNA polymerase beta's closing and active site assembly. *J. Am. Chem. Soc.* **2004**, *126*, 8441–53.
- (29) Florian, J.; Goodman, M. F.; Warshel, A. Computer simulation of the chemical catalysis of DNA polymerases: discriminating between alternative nucleotide insertion mechanisms for T7 DNA polymerase. *J. Am. Chem. Soc.* **2003**, *125*, 8163–77.
- (30) Florian, J.; Goodman, M. F.; Warshel, A. Computer simulation studies of the fidelity of DNA polymerases. *Biopolymers* **2003**, *68*, 286–99.